Voltage-assisted asperity formation in styrene butadiene at room temperature: Cross-linking at the nanoscale

M. Rackaitis,[2] D. Kashyn,[1] E. Rowicka,[1] P. B. Paramonov,[1] R. R. Mallik,[1] and S. F. Lyuksyutov[1,*]
[1]*Department of Physics, The University of Akron, Ohio 44325-4001, USA*
[2]*Bridgestone Americas, Center for Research and Technology, 1200 Firestone Parkway, Akron, Ohio 44317-0001, USA*
(Received 5 May 2008; published 5 August 2008)

Nanoscale surface modification is reported for styrene butadiene rubber using an electrically biased conducting atomic force microscope tip. Under appropriate bias conditions, the local electric field magnitude is of the order of 10^8-10^9 V m^{-1}, which is sufficiently large to initiate cross-linking in the rubber. Peaklike surface features, surrounded by a circular trough and a raised ring, are created by careful and controlled retraction of the biased tip. The features' aspect ratios can be controlled by modifying the tip retraction protocol, tip geometry, and bias voltage. Typical feature dimensions reported here vary from approximately (0.5–10)-nm high and up to several hundreds of nanometer in diameter. Although the temperature of the rubber is above the glass transition and the rubber is in a viscous state, the features are stable over a period of several days once created—which is believed to be due to cross-linking of the rubber during feature formation. Modeling of the electric field distribution in the vicinity of the tip is presented, which strongly supports the assertion that the resulting nonuniform electric field induces nanostructure formation and initiates cross-linking. A mechanism is proposed whereby source material is redistributed in the proximity of the tip/surface region to form the observed features.

DOI: 10.1103/PhysRevB.78.064201 PACS number(s): 61.25.hk, 68.37.Ps, 81.16.Rf, 81.16.Nd

I. INTRODUCTION

The ubiquity of polymers and polymer-based materials in everyday life arises from important commercial applications at the macroscale. For example, the tire industry utilizes synthetic rubber made from polymerization of different monomers—to their versatility in diverse applications at the nanoscale, such as displays, sensors, optoelectronics, and polymer data storage.[1–4] The influence of an external electric field on the stability of polymer surfaces is a very active area of research. This includes electrohydrodynamical instability (EHD)[5] and surface fluctuations[6] using mask techniques, nanoelectrochemistry,[7] and also nanoscopic mass transport on the microsecond time scale using atomic force microscopy-assisted electrostatic nanolithography (AFMEN)[8] in various films although polymer films have been the most intensively studied up to date. AFMEN has been shown to generate routinely (1–50)-nm-high and (10–100)-nm-wide features by inducing an electric breakdown between a sharp (20–40)-nm asperity, such as an atomic force microscope (AFM) tip and attoliters of substances such as dielectrics (polystyrene and polymethylmethacrylate), semiconductors (*a*-Si, CdS),[9] self-assembled alkylthiolate monolayers,[10] and also in bio-materials such as *Iridovirus Wiseana*.[11]

It is important to understand and differentiate fundamental physical processes occurring under extreme conditions when the applied electric filed exceeds 10^8-10^9 V m^{-1} in small volumes (10–100 al) of condensed matter. These processes may include—but are not limited to—fast overheating of molecules, electrochemistry in small volumes, mass transport, and, in case of macromolecules, electrically induced cross-linking at the nanoscale. To limit the number of physical factors, in this work we have selected styrene butadiene rubber (SBR). SBR is a widely used polymer in the rubber industry. Depending on the styrene content, the SBR glass transition temperature (T_g) can vary over a range typically between −80 and −30 °C. At room temperature SBR behaves as a polymeric liquid, which eliminates the need to heat it above the glass transition point. Due to the liquid nature of SBR (namely, fast molecular relaxation), the formed features are short lived—making standard AFM measurements of SBR almost impossible.

The major goal of this study is to show that it is possible to create very stable features on a polymeric liquid surface. As we will show, these features are associated with cross-linking of macromolecules in small volumes of SBR. Two additional goals are: (1) to solve the distribution of electrostatic field and field gradient in the tip-surface junction using Laplace equation and (2) to study the topological peculiarities of nanostructure formation associated with nonuniformity of the induced electric field.

II. EXPERIMENT

In order to negate SBR molecular mobility at room temperature, samples were prepared from SBR solution mixed with standard rubber cross-linking agents to induce cross-linking of SBR molecules, which normally occurs at temperatures above 110 °C. Thermal cross-linking of SBR molecules without additional cross-linking agents is also possible at higher temperatures.[12] The SBR solution was prepared through the following steps: Commercial SBR from the Firestone Synthetic Polymer Co. was used as the starting product (Duradiene 706 with a molecular weight of about 150 kg/mol, styrene content of 23.5%, vinyl-1,2 content of 12%, and T_g of about −62 °C). Approximately 40 g of the SBR was mixed with 0.37 g of antioxidant (Santoflex-13), 0.8 g of stearic acid, 3.8 g of aromatic oil, 0.57 g of sulfur, 0.57 g of diphenyl guanidine (DPG), and 0.68 g of

N-cyclohexyl benzothiazole sulfenamide (CBS). An antioxidant was added in order to protect the SBR from degradation. Stearic acid and oil are processing aids that facilitate better dispersion of the ingredients in the rubber and sulfur. DPG and CBS are curatives that afford a better degree of control over cross-linking.[12] Mixing was performed using a 65 g Brabender mixer at mixing speed of 60 rpm and the mixing temperature was maintained at 100 °C. Approximately 5 g of mixed compound was dissolved in 0.5 liter of toluene producing a 0.01 wt% solution from which SBR were spin coated onto silicon substrate.

The SBR solution was spun cast at 2000–6000 rpm for 20–40 s onto optically flat silicon substrates to produce films with thicknesses between 2 and 100 nm. The roughness of the silicon surface was estimated to be less than 0.5 nm and the SBR film thickness was analyzed using AFM. For AFM measurements, films were gently scratched using a sharp stylus and the profile of the scratch was measured using standard AFM procedure. Commercial software provided by the manufacturer (Veeco Metrology) was used to calculate average film thickness. Several areas of the films were dewetted due to poor adhesion of SBR to silicon, thus providing additional areas of film thickness measurement. The measurements of scratched and dewetted areas yielded similar film thickness values.

In this study two Veeco Metrology 3100 Dimensions AFMs were employed. One of these (a Nanoscope III) was for surface characterization and the other (a Nanoscope IV) for surface patterning. The following conductive noncontact MikroMasch tips were used to pattern nanostructures in SBR films: (1) normal type with force constant 5 N m^{-1}, tip diameter 20 nm, and resonance frequency 240–330 KHz; and (2) sharp type with force constant 5 N m^{-1}, tip diameter 5 nm, and resonance frequency 160 KHz. In any separate experiment, the tip was mounted on a tip holder and isolated from electrical parts of the AFM by a piece of isolating tape. Nanostructures were formed using *z*-lift amplitude modulated (ZAM) protocol running C++ combined with DIGITAL INSTRUMENTS nanolithography package. There are four basic steps for tip manipulation through ZAM: (1) The tip is brought close to the surface to a distance at which the amplitude of tip vibration was damped by three orders of magnitude—as monitored through tip vertical deflection signal using Textronics oscilloscope. This tip-sample distance was selected as reference point. (2) The oscillating tip is then raised to a distance varied between 1 and 10 nm (Level I). (3) A bias voltage (negative or positive) in the range 1–40 V is applied to the tip as it is retracted to a distance varied between 10 and 1000 nm (Level II). The speed of the tip retraction varied between 50 and 100 nm s^{-1}. (4) The tip is moved laterally to another position above the surface and steps (1)–(3) are repeated to create more structures in a similar manner. ZAM protocol is shown schematically in Fig. 1.

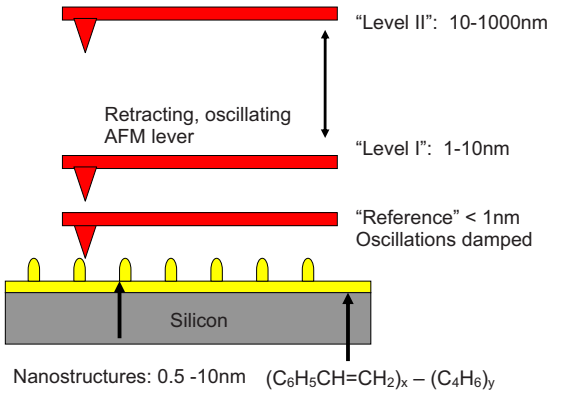

FIG. 1. (Color online) ZAM protocol: Step 1: An unbiased oscillating AFM cantilever is brought to the surface of an SBR film [(4–100)-nm thick] and oscillations are damped by three orders of magnitude. Step 2: The cantilever is retracted to Level I above the reference point between 1–10 nm from the surface. Step 3: A bias voltage (varied between −1 and −40 V) is applied to the cantilever, which is then lifted from the Level I to Level II (10–1000 nm from the surface) at a speed between 50 and 100 nm s^{-1}. Nanostructures (dots or circular rings) are patterned on the SBR surface. Step 4: The cantilever is laterally displaced to another point (typically between 10–500 nm from the original starting point) and steps 1–3 are repeated.

III. RESULTS AND DISCUSSION

An example of a 10×10 dot array, patterned in a 50-nm-thick SBR film using ZAM protocol, is shown in Fig. 2. The height of the dots varies between 1 and 3 nm. The whole array was created in 170 s. It was found that the structures of this particular array remained unchanged for 48 h of monitoring. The stability of the structures was further investigated by monitoring the dimensions of the nanostructures formed in the SBR films under variable conditions. Variables included are: exposure time (which was varied between 0.1 and 5 s), tip retraction distance from the reference point (varied between 1 and 1000 nm), tip bias (varied between −1 and −40 V), and the type of AFM tip (two were used—one with a 5 nm radius and the other 20 nm). A set of samples of different thickness was investigated in this study.

The minimum thickness of the SBR films studied was 4 nm and the maximum thickness was 100 nm. It was found that the bias voltage and tip sharpness (determined by the tip diameter) were the two most critical factors affecting the stability of the nanostructures patterned in the SBR films. Graphs illustrating the stability of the nanostructure's height and width, over a period of approximately one week, are shown in Fig. 3. It was observed that two kinds of features formed with ZAM protocol remained stable while the surrounding areas of SBR (that were not exposed to electric field) were subject to change.

A schematic presentation of an AFM tip above SBR surface is depicted in Fig. 4. The tip is presented as a hyperboloid with apex radius, *R*, separated from the polymer surface by a distance *t*. Biasing the tip produces a nonuniform electric field, which in turn is capable of reshaping the polymer medium in question.

The distribution of electrostatic potential, field, and field gradient in the tip-surface junction was calculated from a numerical solution of the Laplace equation using axially symmetric cylindrical (r,z) coordinates:

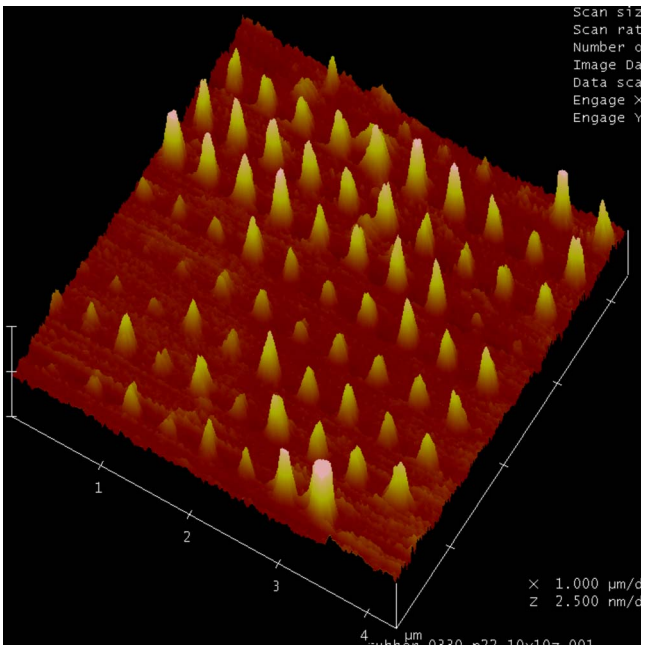

FIG. 2. (Color online) A fragment of a 10×10 array of nanodots (240-nm wide and 3-nm high) formed on a 50-nm-thick SBR film using ZAM protocol with a tip bias voltage in the range−10–−15 V. The tip was retracted from the "reference" point to a point 100 nm higher over a period of 1 s at speed of 100 nm/s). The nanodots remained intact over an observation period of 48 h.

$$\frac{\partial^2\varphi}{\partial r^2}+\left[\frac{1}{r}+\frac{1}{\varepsilon}\frac{\partial\varepsilon}{\partial r}\right]\frac{\partial\varphi}{\partial r}+\frac{1}{\varepsilon}\frac{\partial\varepsilon}{\partial z}\frac{\partial\varphi}{\partial z}+\frac{\partial^2\varphi}{\partial z^2}=0, \tag{1}$$

where $\varphi(r,z)$ and $\varepsilon(r,z)$ are the position-dependent electrostatic potential and the dielectric permittivity, respectively. The equipotential surface of the tip and the grounded plane at $z=0$ provide boundary conditions for Eq. (1). Finite difference discretization with a successive over-relaxation (SOR) method[13] was used to calculate the potential $\varphi(r,z)$, the magnitude of the (external) electric field,

$$E(r,z)=\sqrt{\left(\frac{\partial\varphi}{\partial r}\right)^2+\left(\frac{\partial\varphi}{\partial z}\right)^2}, \tag{2}$$

and the field induced pressure gradient (ponderomotive force density):[14,15]

$$\nabla p(r,z)=-\frac{\varepsilon_0}{6}(\varepsilon-1)(\varepsilon+2)\,\nabla E^2(r,z). \tag{3}$$

Representative contour plots for the resulting electrostatic potential and field are presented in Fig. 4. The numerical accuracy of the finite difference calculations was verified by comparison to an analytical solution for an electric field of a hyperboloidal tip in the absence of a dielectric film.[16]

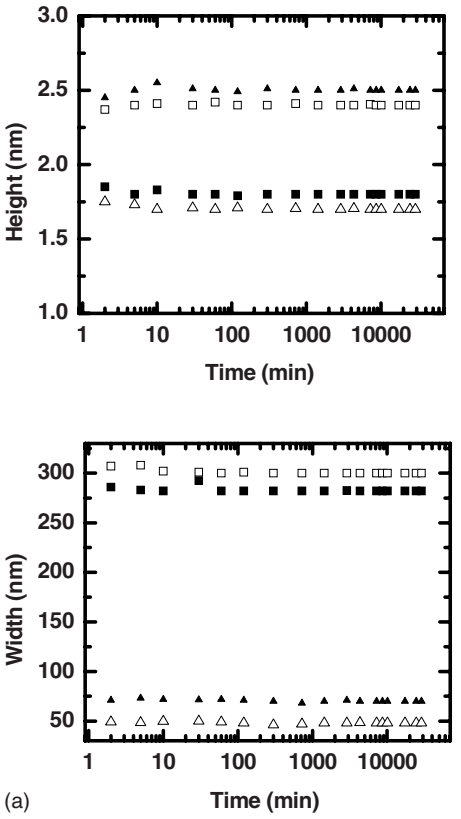

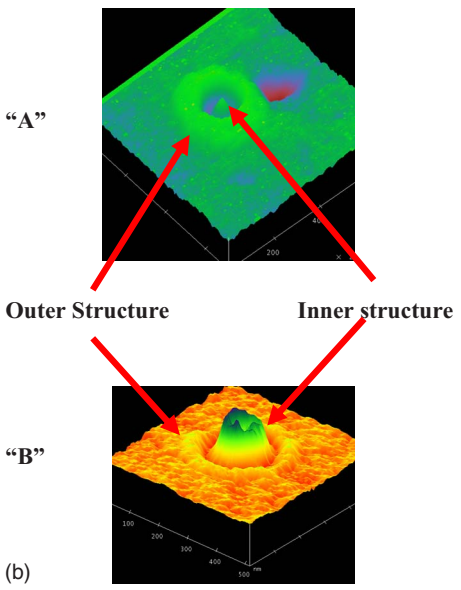

FIG. 3. (Color online) Dependence of the (a) height and (b) width of two types ("A" and "B") of nanostructures formed on SBR versus time. Type A—open triangles correspond to inner structure and open squares correspond to outer structure (ring); The bias voltage was −25 V and the exposure time was 0.5 s; Type "B"—closed triangles correspond to inner structure and closed squares correspond to outer structure (ring); The bias voltage was −25 V and the exposure time was 1.5 s. (c) 3D images of types A (upper image) and B (bottom) nanostructures.

Equation (1) was solved using typical values of the experimental parameters employed for the materials under investigation. These are as follows: SBR dielectric permittivity

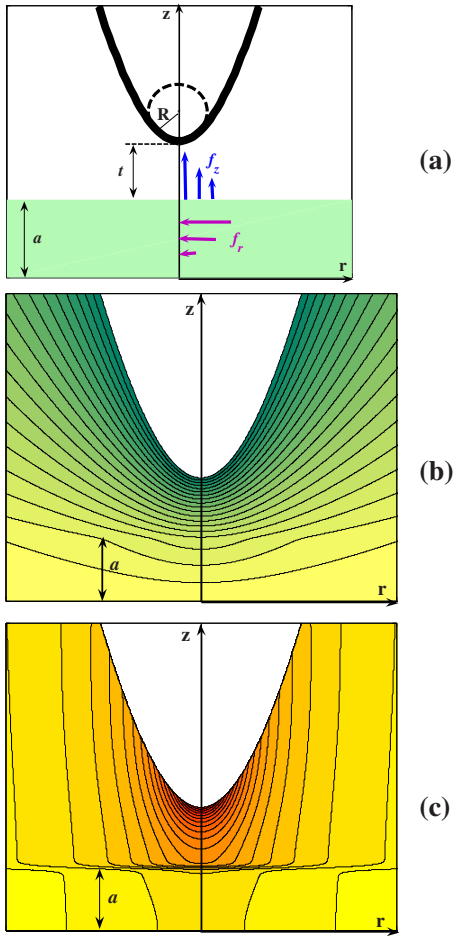

FIG. 4. (Color online) (a) Schematic presentation of an axially symmetric AFM tip—SBR surface junction. The AFM tip is approximated as a hyperboloid with an apex radius, R. The tip-surface separation, t, and SBR film thickness, a, are also shown. The radial, f_r, and axial, f_z, components of the ponderomotive force, $\vec{f}=-\nabla p$, are responsible for the reshaping of the polymer medium and the formation of nanostructures. Representative contour plots for (b) electrostatic potential $\varphi(r,z)$ and (c) electric field $E(r,z)$.

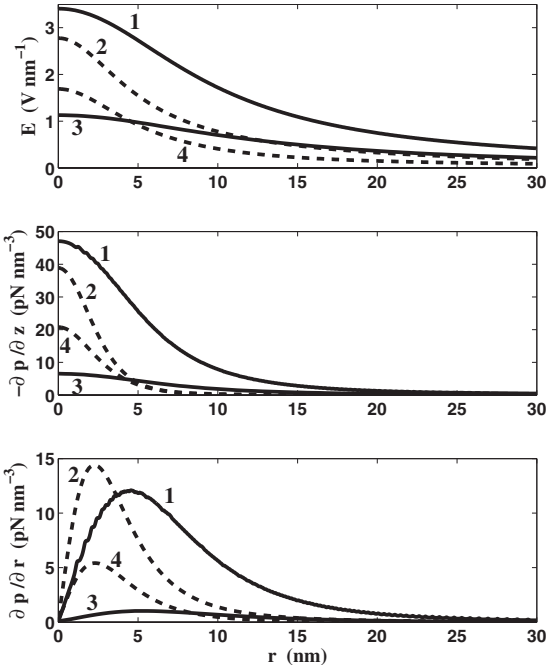

FIG. 5. The variation of the electric field E and the pressure gradient components, $\partial p/\partial z$ and $\partial p/\partial r$, evaluated near polymer surface (1 nm below $z=a$) with respect to the radial coordinate r for the cases of thin (curves 1 and 2, $a=4$ *nm*) and thick (curves 3 and 4, $a=100$ nm) SBR films. Solid and dashed lines correspond to normal ($R=20$ nm) and sharp ($R=5$ nm) AFM tips, respectively. Note: larger values and longer radial extension of the pressure gradient components are observed for the case of a thin polymer film.

$\varepsilon=2.5$, SBR film thickness $a=4$ or 100 nm, tip-surface distance $t=1$ nm, tip bias voltage $U=20$ V, and tip radius $R=20$ (normal) or 5 nm (sharp). The calculated electric field [Eq. (2)] and pressure gradient [Eq. (3)] applied to a polymer film in the proximity of the film surface are presented in Fig. 5 as a function of the radial coordinate r. A comparison of thin (4 nm) and thick (100 nm) polymer films indicates larger magnitudes and a longer radial extent of the pressure gradient components (ponderomotive forces) in the case of a thin film. In particular, the *radial* component of the pressure gradient [Eq. (3)] is stronger and is acting over a larger area in thin films. These observations are not affected by variations in the AFM tip radius between 5 (sharp) and 20 nm (normal).

To compare the results of modeling with experiment, the sets of features were formed in SBR films at various field strengths using AFM tips of two different sharpnesses. The tips used have the following characteristics: Standard silicon tips, covered with gold, and tip radius $R=20$ nm; and sharp tungsten tips—manufacturer's product code DP14/HI'RES-W with resonant frequency 160 KHz—force constant 5 N m^{-1}, and tip radius $R=5$ nm. A comparison of the features formed using the standard versus sharp tips, for different magnitudes of electric field (as determined by bias voltage and tip-surface separation), is presented in Fig. 6. As can be seen, a trend is observed for the magnitude and structure of the features with increasing bias voltage for a given tip-surface separation. One can see that the features form initially as single dots [Figs. 6(a)–6(c), corresponding to bias voltages of −8, −15, and −20 V, respectively] and their shape gradually changes from dots to protrusions directly under the AFM tip as the bias increases. One also observes that the features' dimensions grow in height and width with increasing bias. At some threshold tip bias, typically−24–−25 V for a standard tip and −13−−15 V for a sharp tip, a ring of elevated material forms around the central peak. Figure 6(d) shows features formed at a bias of −25 V for a normal tip, while Figs. 6(e)–6(h) corresponds to features formed at voltages of −15, −20, −25, and −30 V, respectively, for a sharp tip. Nanostructure dimension may exceed the tip size and the lateral extent of the electric field, which was observed earlier,[8,11] and is most likely related to viscoelastic response of polymeric media.[12,17]

Our calculations indicate that in the case of thin polymer films, the radial pressure gradient [Eq. (3)] is stronger for the sharp tip than for the standard tip biased with the same voltage. This could explain why electric voltage-assisted asperities (EVA), formed in thin SBR films as the polymer medium

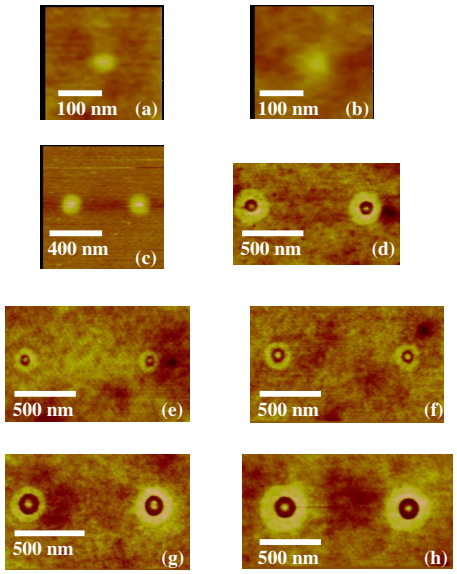

FIG. 6. (Color online) Comparison of raised nanostructures patterned on a 10-nm SBR film using ZAM protocol (ZAM lift up from 1 to 100 nm.) with two different tips. [(a)-(d)] "Standard" tip with radius 20 nm. (a) A 45-nm-wide and 1.4-nm-high dot; The tip bias was −8 V. (b) A 51-nm-wide and 1.2-nm-high dot; tip bias was −15 V. (c) A 118-nm-wide and 3.0-nm-high dot; tip bias was −20 V. (d) Two concentric rings 307-nm wide: The central peak and the outer ring are 1.6-nm high; The tip bias was −25 V. [(e)-(h)] "Sharp" tip with diameter 5 nm. (e) Two concentric rings 200-nm wide: The central peak and the outer ring are 0.9-nm high; The tip bias was −15 V. (f) Two concentric rings 240-nm wide: The central peak is 1. 6 nm and the outer ring is 0.7-nm high; Tip bias was −20 V; (g) Two concentric rings 330-nm wide: The central peak and the outer ring are 1.7-nm high; Tip bias was −25 V; (h) Two concentric rings 420-nm wide: The central peak and the outer ring are 1.5-nm high; Tip bias was −30 V.

flows toward the tip position ($r=0$), can be induced at a lower bias (-13–-15 V) for the sharp tip ($R=5$ nm) than for the standard tip ($R=20$ nm), which requires a bias voltage of −25 V.

It was established that no features are formed when the tip bias was less than −5 V for either the sharp or standard tip and for tip-sample separations between 1 and 100 nm. This suggests that nanostructures are not stable when a small bias is used, and they disappear as molecular relaxation minimizes the surface tension. As the voltage was increased in magnitude above −8 V, the observed stable features were formed on SBR surface, which suggests a field threshold for nanostructure stabilization due to a field induced chemical cross-linking. An order of magnitude estimate of the electric field sufficient to initiate SBR cross-linking can be obtained assuming that the polarization energy stored in a molecular volume has to be as high as the π-bond strength $D \sim 282$ kJ/mol. Such an estimate results in the following threshold field:

$$E_{\text{th}} = \sqrt{\frac{2D\rho}{\varepsilon_0(\varepsilon - 1)M}}, \tag{4}$$

where ρ and M are the mass density and molecular weight, respectively. The threshold field evaluated using material parameters of SBR described in the experimental section is about 0.5 V/nm, which, according to our calculations (Fig. 5), is attained under typical experimental conditions. While polymer surface tension may play an important role in the initial stage of nanostructure formation, it does not result in any significant topographical changes once the cross-linking was induced, and the nanostructures remain very stable as presented in Fig. 3.

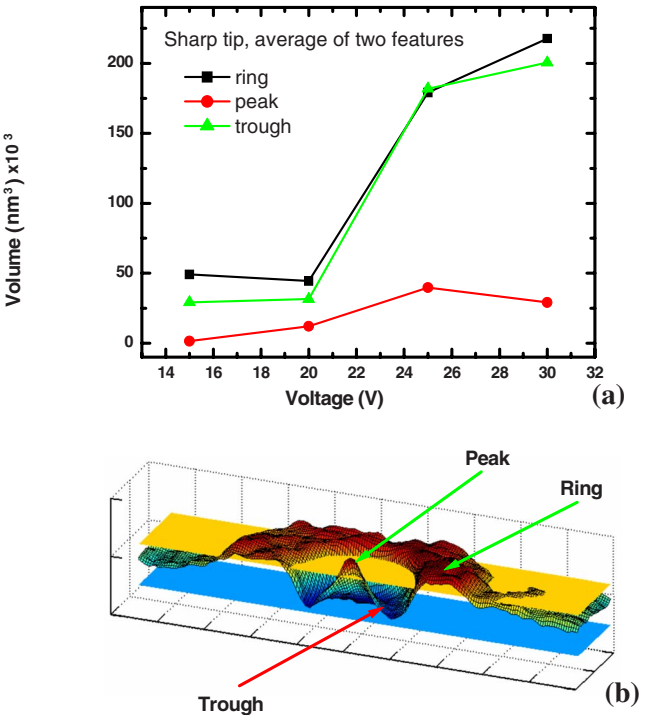

FIG. 7. (Color online) (a) Feature element volume dependence on applied voltage; (b) illustration of volume measurement from AFM image. The feature is bisected for clarity. The ring volume was calculated as the volume between the yellow intersecting plane and the measured surface. The peak volume was calculated as the volume between the blue intersecting plane and measured peak surface. Trough volume was determined by calculating the volume below the intersecting plane (not shown) going through the average height of the ring and measured surface.

The formation of topological peculiarities, ring(s) around a single peak, could be mostly associated with the geometrically nonuniform mass transport due to the competition between electric-field distribution and the thickness of the SBR film. As indicated above, the radial component of the pressure gradient acting on the polymer film is stronger for thin films and could be one of the factors responsible for a trough ring nanostructure formation. To evaluate the mass transport of material under the AFM tip, the volume of displaced SBR was calculated using data extracted from the AFM images. The calculations were performed using WSxM software.[18] The features' characteristics can be defined as being comprised of a central peak circumscribed by a trough region, which is in turn surrounded by a ring of raised material as shown in Fig. 7(b). Figure 7(a) shows the corresponding dependence of the volume change in each feature component (i.e., the peak, trough, and ring) with bias voltage for features created using the sharp tip (5 nm). Every data point is cal-

culated from at least three different features and the average is presented in this plot. In order to calculate the volume of the components of features, the image data was intersected with reference planes at specific levels—as indicated in Fig. 7(b). The yellow plane is assumed to be at the average surface height and the blue plane is at a depth corresponding to the bottom of the trough. Using these reference planes, we define the volume of the ring as its volume lying above the yellow plane, while the volume of the peak is its volume above the blue plane. The trough volume was defined as its volume enclosed between the yellow and blue planes. As can be seen from the Fig. 7(a), the ring and trough volumes are very similar, supporting the hypothesis of mass redistribution by the electric field. It also shows that there is a little or no polymer ablation. The peak volume does not change significantly, which shows that there is no influx of material to the peak region and that the trough is as deep as the film thickness.

Analysis of the peak formation using the normal tip shows that the peak volume increases with increased voltage. The difference between the ring and trough volumes is greater for features produced by the normal tip. Analysis of peaks formed on thick films shows that—in the range of investigated voltages—it has not been possible to form peak-ring type features, which suggests that the main process governing feature formation is mass transport in the electric-field region.

Figure 8 illustrates the explanation for this conclusion. Peaks are formed at the initial stage of the process and as it proceeds further deformation of the polymer film surface occurs under the AFM tip. This deformation is possible because the polymeric liquid behaves as a non-Newtonian fluid[12,17] in the region around the formed peak. In order to support continuous peak growth, material has to be drawn from beneath the peak or the surrounding area. In the case of thick films, there is enough material beneath the peak such that there is no significant increase in the peak's width under the investigated field strengths. However, in case of thin-film samples, deformation of the polymeric film surface leads to a redistribution of material around the peak and there is an insufficient source of available polymer to support the quick growth of the peak. As a result, the material surrounding the depleted region is drawn instead to form the peak. It is also observed that the outer diameter of the trough varies only by about 150 nm (from 250 to 400 nm) for ring peak features formed by a sharp tip ring peak and that the features beside the outer rim of the trough becomes steeper with increasing voltage. This shows that the material from which the ring is formed comes from the trough area and the area surrounding the ring. This could also explain the weak dependence of trough outer diameter on applied electric-field strength.

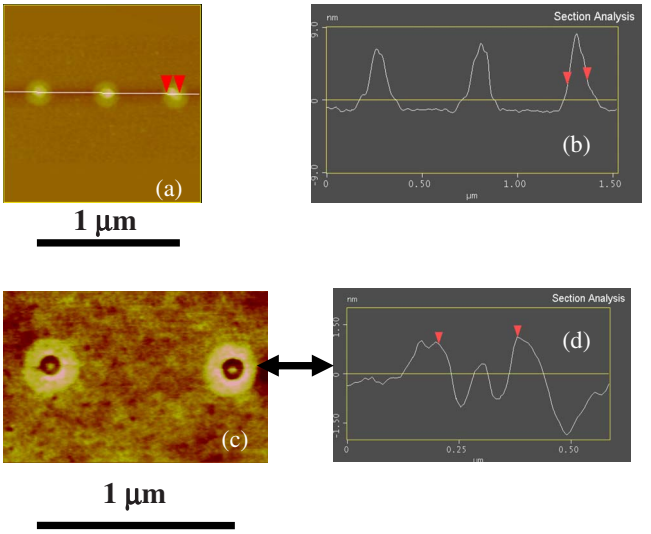

FIG. 8. (Color online) Comparison of nanostructure formation in thick versus thin SBR films. [(a)-(b)] 100-nm-thick SBR film (7-nm-high and 105-nm-wide dots). [(c)-(d)] 4–nm-thin SBR film (1.25-nm–high and 170-nm-wide dots).

IV. SUMMARY

The data presented here show that it is possible to create stable surface features on an essentially liquid surface where natural molecular relaxation rates are much higher than that of AFM measurement capabilities. However, it has also been demonstrated in the past that nanostructures can be patterned in such polymer films as polystyrene and poly(methylmethacrylate) due to the plastic deformation of the surface at the nanoscale.[19] The fact alone that the surface features are observed proves that cross-linking of SBR molecules has occurred. An abundance of experimental data collected in this work indicates the cross-linking in SBR at the nanoscale in the presence of an electric field of sufficient magnitude. The AFMEN technique[8] is particularly well suited for the creation of the observed surface features as it has the capability to provide extreme (10^8–10^9 V m^{-1}) localized electric fields, which cannot be easily obtained otherwise. Results show that the geometry of the observed features, formed by cross-linking of SBR under an AFM tip, depends on the applied electrostatic field strength. Furthermore, the features remain intact for long periods of time.

*Corresponding author. sfl@uakron.edu

[1] K. S. Lee, *Polymers for Photonic Applications: Nonlinear, Optical, and Electroluminescence Polymers* (Springer, New York, 2002).

[2] T. Tervoort and C. Weder, *Polymers in Display Applications*, Macromolecular Symposium No. 154 (Wiley, New York, 2000).

[3] N. Akmal and A. Usmani, *Polymers in Sensors: Theory and Practice* (Oxford University Press, New York, 1998).

[4] P. Vettinger, M. Despont, U. Drechsler, U. During, W. Haberle, M. I. Lutwyche, H. E. Rothuizen, R. Stutz, R. Widmer, and G. K. Binning, IBM J. Res. Dev. **44**, 323 (2000).

[5] E. Schaeffer, T. Thurn-Albrecht, T. P. Russell, and U. Steiner,

Nature (London) **403**, 403 (2000).
[6] K. A. Leach, Z. Lin, and T. P. Russell, Macromolecules **38**, 4868 (2005).
[7] S.-Y. Jang, M. Marquez, and G. A. Sotzing, Synth. Met. **152**, 345 (2005).
[8] S. F. Lyuksyutov, R. A. Vaia, P. B. Paramonov, S. Juhl, L. Waterhouse, R. M. Ralich, G. Sigalov, and E. Sancaktar, Nat. Mater. **2**, 468 (2003).
[9] I. Dolog, R. R. Mallik, and S. F. Lyuksyutov, Appl. Phys. Lett. **90**, 213111 (2007).
[10] P. B. Paramonov, S. F. Lyuksyutov, O. V. Mayevska, M. A. Reagan, R. A. Vaia, S. Juhl, K. Umemura, H. Tobari, and M. Hara, Langmuir **22**, 6555 (2006).
[11] S. F. Lyuksyutov, Curr. Nanosci. **1**, 245 (2005).
[12] R. I. Taner, *Engineering Reology* (Clarendon, Oxford, 1985).
[13] G. Birkhoff and R. E. Lynch, *Numerical Solution of Elliptic Problems* (SIAM, Philadelphia, 1984).
[14] L. D. Landau and E. M. Lifshitz, *Electrodynamics of Continuous Media* (Pergamon, New York, 1960).
[15] W. R. Smythe, *Static and Dynamic Electricity* (McGraw-Hill, New York, 1968).
[16] J. D. Zuber, K. L. Jensen, and T. E. Sullivan, J. Appl. Phys. **91**, 9379 (2002).
[17] R. B. Bird, R. C. Armstrong, and O. Hassager, *Dynamics of Polymeric Liquids*, 2nd ed. (Wiley, New York, 1987).
[18] I. Horcas, R. Fernandez, J. M. Gomez-Rodriguez, J. Colchero, J. Gomez-Herrero, and A. M. Baro, Rev. Sci. Instrum. **78**, 013705 (2007).
[19] S. F. Lyuksyutov, P. B. Paramonov, R. A. Sharipov, and G. Sigalov, Phys. Rev. B **70**, 174110 (2004).